

Improving ALD- Al_2O_3 Surface Passivation of Si Utilizing Pre-Existing SiO_x

Michael N. Getz , Marco Povoli , and Eduard Monakhov 

Abstract— Al_2O_3 has rapidly become the surface passivation material of choice for $p+$ layers of solar cells because of its high negative fixed charge, good long-term and thermal stability, and no parasitic absorption. In this article, the surface saturation current density, fixed charge, and interface state density are compared for Al_2O_3 deposited on Si substrates where the pre-existing out-of-the-box SiO_x layer was not removed, with substrates where the SiO_x was removed by hydrofluoric acid. The depositions are performed by atomic layer deposition at temperatures in the 150–300 °C range, using trimethylaluminum, H_2O , and O_3 as precursors. The samples where the native oxide was not removed achieve a higher level of surface passivation for every tested deposition temperature, with the sample deposited at 200 °C exhibiting a surface saturation current density of only 0.9 fA/cm² after annealing, a fixed charge of $-4.2 \times 10^{12} \text{ cm}^{-2}$, and a density of interface states of $9.8 \times 10^9 \text{ cm}^{-2} \text{ eV}^{-1}$. Capacitance and conductance voltage characteristics reveal a strong correlation between the surface saturation current density and the density of interface states and fixed charges. It is also determined that the long-term stability of the surface passivation depends on the deposition temperature, with higher deposition temperatures resulting in improved long-term stability. The results indicate that H-terminated Si prior to Al_2O_3 deposition may have a detrimental effect on the surface passivation.

Index Terms— Al_2O_3 growth rate, effect of HF-dip, long-term stability Al_2O_3 , optimal deposition temperature Al_2O_3 , out-of-the-box silicon oxide, surface passivation, TMA + O_3 + H_2O ALD.

I. INTRODUCTION

A Al_2O_3 deposited by either atomic layer deposition (ALD) or plasma-enhanced chemical vapor deposition (PECVD) has become the industry material of choice for surface passivation of commercial Si solar cells [1], because of its high negative

fixed charge being suitable for passivating p -type or lowly doped n -type Si [2]–[8], while also exhibiting excellent thermal, long-term, and UV-stability [9], [10]. The PECVD- $\text{Al}_2\text{O}_3/\text{SiN}_x$ stack is currently dominating the market, however, ALD- Al_2O_3 with PECVD SiN_x capping layer is gaining market shares and is projected to have an almost 50% market share by 2025 [1].

While the origin of the negative fixed charge in Al_2O_3 has been studied rigorously, it still remains a matter of debate. Dicks *et al.* [11] have shown that both oxygen interstitials and aluminum vacancies form stable deep acceptor levels in oxygen-rich environments. These states could potentially be filled by electrons tunneling from Si through the 0.5–2 nm SiO_x that forms at the Si- Al_2O_3 interface [2], [12], [13], and hence become negatively charged. However, Hiller *et al.* [14] have performed calculations showing that replacing Si atoms in the SiO_x layer with Al also results in acceptor levels with energies below the valence band-edge of Si [15], and thus may be an alternative or complementary cause for the fixed negative charge associated with Al_2O_3 . The number of trapped electrons in the SiO_x - Al_2O_3 interface layer has previously been shown to be $>10^{12} \text{ cm}^{-2}$ [3], [16]–[18], implying that the electron concentration near the surface region of silicon is significantly reduced, thereby sharply reducing the probability of electron-hole recombination [19].

Annealing at >400 °C in N_2 , forming gas (FG), or O_2 , reduces D_{it} from $>10^{12} \text{ eV}^{-1} \text{ cm}^{-2}$ to $<10^{11} \text{ eV}^{-1} \text{ cm}^{-2}$ [3], [16]–[18], commonly attributed to either hydrogen diffusion toward the Si- SiO_x interface passivating the Si dangling bonds near the surface and in the bulk, or by increased SiO_x formation between Si and Al_2O_3 [2]–[4], [20], [21]. However, Dingemans *et al.* [22] previously observed similar D_{it} and increased negative fixed charge density when using O_3 or O_2 plasma instead of H_2O as oxidants during the ALD deposition of Al_2O_3 . Later, von Gastrow *et al.* [23] reported that films prepared using H_2O contain significantly more interfacial hydrogen and less carbon, indicating that the role of hydrogen in the surface passivation of Si using Al_2O_3 is complicated. The lowest surface recombination velocities were achieved when using a combination of H_2O and O_3 , which resulted in higher hydrogen concentration and less fixed charge than films prepared using only O_3 , but significantly lower carbon concentration and consequently D_{it} [23].

The SiO_x layer that forms between the Al_2O_3 and Si is important for both D_{it} and Q_{fix} formation, and thus critical for the surface passivation of Al_2O_3 . The fixed interface charge can be tuned by changing the thickness of the layer [24], and the hydrogen, carbon, and aluminum concentration, in addition to

Manuscript received October 29, 2021; revised January 26, 2022 and March 16, 2022; accepted April 20, 2022. Date of publication May 11, 2022; date of current version June 21, 2022. This work was supported in part by The Research Council of Norway under Grant 289437. The Norwegian Micro- and Nano-Fabrication Facility, NorFab, was supported by The Research Council of Norway under Project 295864. (Corresponding author: Michael N. Getz.)

Michael N. Getz is with the Department of Microsystems and Nanotechnology (MiNaLab), SINTEF Digital, 0373 Oslo, Norway, and also with the Department of Physics, University of Oslo, 0315 Oslo, Norway (e-mail: michael.getz@sintef.no).

Marco Povoli is with the Department of Microsystems and Nanotechnology (MiNaLab), SINTEF Digital, 0373 Oslo, Norway (e-mail: marco.povoli@sintef.no).

Eduard Monakhov is with the Department of Physics, University of Oslo, 0315 Oslo, Norway (e-mail: eduard.monakhov@uio.no).

This article has supplementary material provided by the authors and color versions of one or more figures available at <https://doi.org/10.1109/JPHOTOV.2022.3169985>.

Digital Object Identifier 10.1109/JPHOTOV.2022.3169985

the Si-O ratio of the layer, are all likely to affect D_{it} and possibly Q_{fix} . Comparing the surface passivation of Al_2O_3 deposited on SiO_x formed in different conditions is likely to lead to increased understanding of how this layer affects the surface passivation. The effect of various pretreatments on the surface passivation of Al_2O_3 has been investigated previously [25]–[30], demonstrating significant differences. However, as these studies do not compare the surface saturation current density, J_{0s} , considered to be the most useful metric to quantify surface passivation of dielectrics with high Q_{fix} [31], it is challenging to establish a general method. However, methods resulting in a thin SiO_x or SiC_x layer forming prior to Al_2O_3 deposition appear to yield better results than when depositing directly on H-terminated Si [25], [30], [32], [33].

Using the $H_2O + O_3$ combination as oxygen precursors, we previously demonstrated superior surface passivation for Al_2O_3 deposited on as-received wafers with a SiO_x layer already present, compared with wafers subjected to a 3 min HF-dip prior to the ALD deposition at 150 °C [32]. In this article, the aim has been to investigate if using an out-of-the-box oxide remains beneficial at higher deposition temperatures, and to determine the optimal process parameters with respect to reducing J_{0s} . We also investigate how the deposition temperature and pretreatment affects the long-term stability.

II. EXPERIMENTAL

The substrates that were used for impedance measurements were cut from single-side polished (SSP) p -type Cz 525 \pm 20 μm $\langle 100 \rangle$ -oriented silicon wafers with a doping level of $1.8\text{--}2.0 \times 10^{16} \text{ cm}^{-3}$ from Siegert Wafer. Half of the substrates received no further pretreatment, referred to as “no-HF” from here on, while the other half of the substrates were submerged in 2% HF solution for 3 min, followed by a ca. 1 min bubble rinse in DI water, referred to as “HF-dipped” from here on. The unpolished side (back side) of all the substrates were contacted with ca. 180 nm Al by thermal evaporation.

For lifetime measurements, 12 cm^2 substrates were cut from double-side polished (DSP) p -type FZ 500 μm $\langle 100 \rangle$ -oriented silicon wafers with a reported resistivity of 5–12 $\text{k}\Omega \cdot \text{cm}$ from Topsil. The manufacturer reports that the wafers are subjected to SC1 ($NH_4OH/H_2O/H_2O_2$, 85 °C, 10 min) and a SC2 ($HCl/H_2O/H_2O_2$, 85 °C, 10 min) cleaning after chemical mechanical polishing before being placed in shipping boxes after some hours. The oxide that forms during the SC1 and SC2 process and later in air will be referred to as a “SC2-last oxide” from here on.

Half of the substrates were subjected to the HF-dip pretreatment, while the other half received no pretreatment. Note that the properties of the Si– Al_2O_3 interface have been shown to be independent of substrate doping [34].

A Beneq TFS-200 ALD reactor was used for the Al_2O_3 deposition by using trimethyl-aluminium (TMA) (99.999%) from Strem chemicals, H_2O , and O_3 , with a pulse duration of 0.4/2/0.4/2/1/2.5 s for 145 cycles of TMA/ N_2 / H_2O / N_2 / O_3 / N_2 , respectively. The depositions were carried out with background pressure of 2 mbar and deposition temperatures of 150 °C,

200 °C, 250 °C, and 300 °C. The depositions were preceded by an *in-situ* 5 min O_3 pretreatment (30 cycles of 1 s O_3 /9 s N_2) at the deposition temperature to remove potential organic contaminants, flush the O_3 line, and improve the surface reactivity toward TMA. For each deposition temperature, one HF-dipped and one no-HF substrate was loaded into the reactor. Each deposition was performed twice, once for the SSP substrates that were only coated on one side, and once more for the DSP substrates that were coated simultaneously on both sides.

The SiO_x and deposited Al_2O_3 film thicknesses were determined with a J. A. Woollam ellipsometer in the 380–890 nm range. The spectroscopic ellipsometry (SE) experimental data of the samples prior to deposition was fitted using the native silicon oxide model provided by the CompleteEASE software, which uses optical constants determined by Herzinger *et al.* [35]. The Cauchy model was used to parameterize the SE data of the films after deposition. Three measurements were performed at different locations on the surfaces of samples. The uncertainty provided in the reported thicknesses reflect the different thicknesses measured across the surface and includes the uncertainties in the fitted values.

Annealing was performed in a tube furnace at 435 °C for 10 min in FG (10% H_2). The temperature at the sample position was monitored with an external thermocouple.

Ca. 180 nm thick circular Al gate electrodes were deposited using shadow masks with hole diameters of ca. 1 mm by thermal evaporation. A contact area of 0.709 mm^2 was deduced from optical microscopy and this value is used for the calculations performed in this article.

The capacitance-voltage (CV) characteristics and conductance-voltage (GV) characteristics were recorded at various probe frequencies in the range of 500 Hz to 250 kHz, with an oscillation voltage of 30 mV using Precision Impedance LCR Analyzer (4284 A, Agilent Technologies) in parallel conductance mode. The samples were briefly illuminated prior to the voltage sweep, which were performed in darkness. The gate voltage was swept at room temperature from depletion (5 V) to accumulation (–3 V) and back again. Note that the presented figures show the G/ω vs. V characteristics, but are referred to as GV characteristics for brevity.

The effective minority carrier lifetimes of the as-deposited and post annealed samples were recorded using a Sinton Instruments WCT-120 with the generalized quasi-static photoconductance (QSSPC) mode for the as-deposited samples, and the transient photoconductance decay (PCD) mode for the annealed samples. The sample stage was kept at 25 °C. The measurements of the annealed samples were performed after the sample temperature cooled down to ca. 25 °C, ca. 10 min after they were extracted from the furnace.

III. RESULTS

The thicknesses obtained by SE for the samples before and after deposition are provided in Table S1 and S2. Because of the similarities in refractive index of SiO_x and Al_2O_3 in the amorphous state, SE measurements will yield the total dielectric thickness [36], the growth per cycle (GPC) presented in Fig. 1

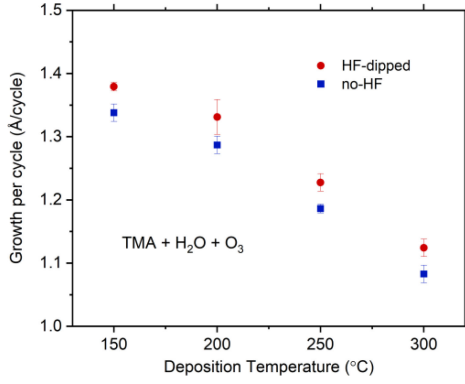


Fig. 1. Growth rates of no-HF and HF-dipped samples at 150°C–300°C for the TMA + H₂O + O₃ process. SE thickness measured using a model for native SiO_x prior to deposition was subtracted from the final thickness before GPC was calculated. Note that for HF-dipped samples, some of the growth may be attributed to additional SiO_x formation during the deposition.

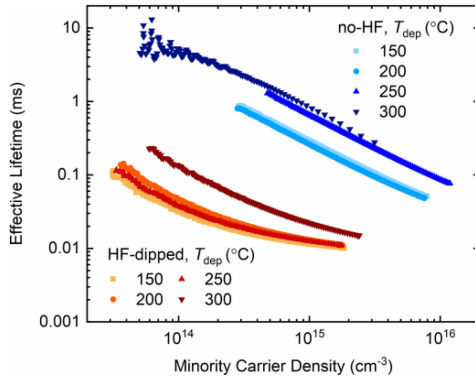


Fig. 2. Effective carrier lifetime of as-deposited HF-dipped (red-scale) and no-HF (blue-scale) samples.

has therefore been calculated for films deposited on SSP substrates after subtracting the thickness measured by SE prior to deposition. There is no literature describing the growth rate of the TMA + H₂O + O₃ system, however, the growth rates are in close agreement with those observed for TMA + O₂ plasma [37], and slightly higher for each temperature than previously observed for just TMA + O₃ [38]. The apparent increased growth rate of HF-dipped samples relative to the no-HF samples is attributed to formation of SiO_x during the initial ALD-cycles, as previously demonstrated by transmission electron microscopy (TEM) [2], [12], [13]. There is little or no significant difference in total film thickness between HF-dipped and no-HF samples when deposited at the same deposition temperature. This indicates that the thickness of the SiO_x layer that forms on HF-dipped samples during the deposition is similar to the SC2-last SiO_x thickness of ca. 1.6 nm (Table S1), provided that little or no further SiO_x is formed on no-HF samples.

A. Lifetime Measurements

The effective lifetime in the as-deposited no-HF and HF-dipped samples is presented in Fig. 2. The no-HF samples consistently exhibit lifetimes at least one order of magnitude longer than the HF-dipped samples for all deposition temperatures,

T_{dep} , over the recorded injection level range. The sample deposited at 300°C exhibits the longest lifetime in the as-deposited state, which is attributed to the deposition temperature having an effect similar to that of annealing.

Post FG annealing, the lifetime improves significantly for all samples, as shown in Fig. 3(a) and (b) for no-HF and HF-dipped samples, respectively. J_{0s} was deduced from the linear fit of the linear region of inverse lifetime data at high injection, shown for no-HF and HF-dipped samples in Fig. 3(c) and (d), respectively, using the Kane–Swanson slope method [39]

$$\frac{1}{\tau_{\text{eff}}} - \frac{1}{\tau_{\text{Auger}}} = \frac{1}{\tau_{\text{SRH}}} + 2 \frac{J_{0s}(N_a + \Delta n)}{qn_i^2 W} \quad (1)$$

where τ_{eff} is the measured effective excess carrier lifetime, τ_{Auger} is the intrinsic Auger lifetime [40], τ_{SRH} is the defect-related bulk lifetime, N_a is the base doping level, Δn is the excess carrier density, q is the elementary charge, n_i is the intrinsic carrier concentration ($8.305 \times 10^9 \text{ cm}^{-3}$ at 298.15 K), and W is the wafer thickness. The no-HF samples exhibit consistently lower J_{0s} at each deposition temperature, suggesting that the findings reported previously at 150°C [32], are valid for all deposition temperatures using this process. The lowest J_{0s} is observed for deposition temperatures of 200°C for both no-HF and HF-dipped, with the no-HF sample exhibiting $J_{0s} = 0.9 \text{ fA/cm}^2$.

Fig. 4 shows how J_{0s} changes for each sample after 8 months of storage while wrapped in Al-foil inside a zip-lock bag in a cleanroom. The corresponding lifetime data used to determine J_{0s} are available in Fig. S1. The surface passivation provided by ALD-Al₂O₃ has previously been reported to be stable over time, and in some cases an improvement over time is observed [3], [10]. The results in this article indicate that the long-term stability depends on the deposition temperature, with lower deposition temperatures resulting in reduced stability. Samples deposited at 150°C and 200°C exhibit increases in J_{0s} on the order of $\sim 50\%$ (see Fig. S2 for accurate values). However, because of the low initial J_{0s} of the no-HF sample deposited at 200°C, this only amounts to a $< 0.4 \text{ fA/cm}^2$ increase and can thus be said to be reasonably stable in absolute terms. For the HF-dipped sample deposited at 250°C, J_{0s} increased by 10%, while for the no-HF sample, J_{0s} was reduced by ca. 25%. For samples deposited at 300°C, J_{0s} was reduced by 33%–40%. The long-term stability shows no clear dependence on the pretreatment, indicating that the observed changes are primarily related to the Al₂O₃ and not to the SiO_x interface layer. No further changes in the lifetime or J_{0s} were observed in the two weeks following the 8 months of storage, indicating that the films have become stable. Annealing an HF-dipped sample deposited at 150°C again after aging had no effect on the lifetime.

Despite the significantly improved surface passivation over time of the samples deposited at 300°C, they still perform worse than samples deposited at 200°C, which appears to be the optimal deposition temperature when depositing on SC2-last SiO_x and taking long-term stability into account. 200°C was also determined to be the optimal deposition temperature for HF-dipped samples, in agreement with previous studies [6], [38], [41].

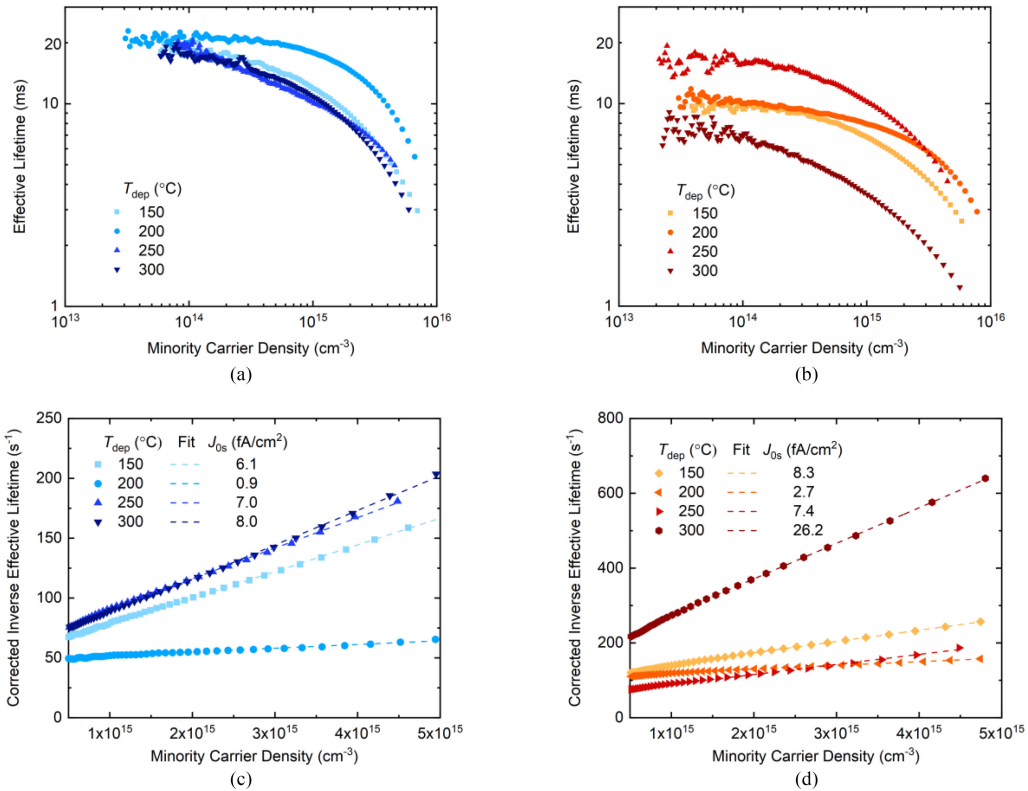


Fig. 3. Effective carrier lifetime vs. minority carrier density of samples deposited at different temperatures post annealing, for (a) no-HF and (b) HF-dipped, and corresponding Auger-corrected inverse lifetime for (c) no-HF and (d) HF-dipped, fitted with a linear fit (dashed lines) from which J_{0s} was calculated from the slope using (1).

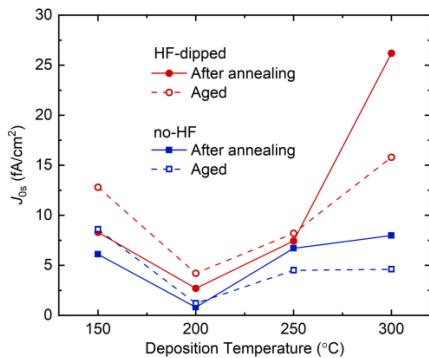


Fig. 4. J_{0s} for each deposition temperature for HF-dipped and no-HF samples, 10 min after anneal (filled), and after storing for ca. 8 months in a cleanroom (open).

B. Capacitance-Voltage and Conductance-Voltage Characteristics

Q_{fix} and D_{it} were estimated from impedance measurements using parallel conductance mode. Series resistance correction was performed according to the method described in the supplementary material. Fig. 5(a) and (b), respectively, show the corrected CV and GV characteristics of the no-HF sample deposited at 200 °C in the as-deposited state, while the CV and GV characteristics of the annealed sample are presented in Fig. 5(c) and (d), respectively. Q_{fix} can be approximated to be equal to

the effective charge, Q_{eff} , obtained from CV characteristics, provided that the contribution from fixed charges is much larger than contributions from other charges. These can be chargeable traps near the Si-Al₂O₃ interface, traps near the Al₂O₃/Al-gate, and mobile charges in the Al₂O₃ [42]. The frequency response of the chargeable traps cause an apparent shift in the flatband voltage, V_{FB} , at low frequencies, while at high frequencies (hf), the filling and emptying of interfacial traps are too slow to follow. If D_{it} is low, then the apparent effect of chargeable traps on V_{FB} can be neglected at high frequencies, however, if D_{it} is high, it will have a significant effect. The as-deposited samples contain a large number of interfacial traps, as evidenced by the hump in the CV characteristics. A similar hump was previously observed for Al₂O₃ prepared using O₃ [36]. The highest frequency used in this article, 250 kHz, was not sufficient to completely avoid apparent contributions from interfacial traps. However, considering the clear exponential dependence of V_{FB} on the frequency in Fig. 5(a), it is possible to estimate Q_{eff} for a given frequency by fitting the resulting data points to a double exponential [32]. Using this approach and letting f approach infinity for the data in Fig. 5(a), $Q_{eff}(hf) \approx -4.6 \cdot 10^{12} \text{ cm}^{-2}$ is obtained (fit is available in Fig. S3). The contribution from mobile or trapped charges can be estimated from the hysteresis that arises by first sweeping the voltage from inversion to accumulation and then back again to inversion at 250 kHz (shown for the no-HF sample deposited at 200 °C, post annealing, in Fig. S4). For the as-deposited samples, the hysteresis at C_{FB} is in the range of

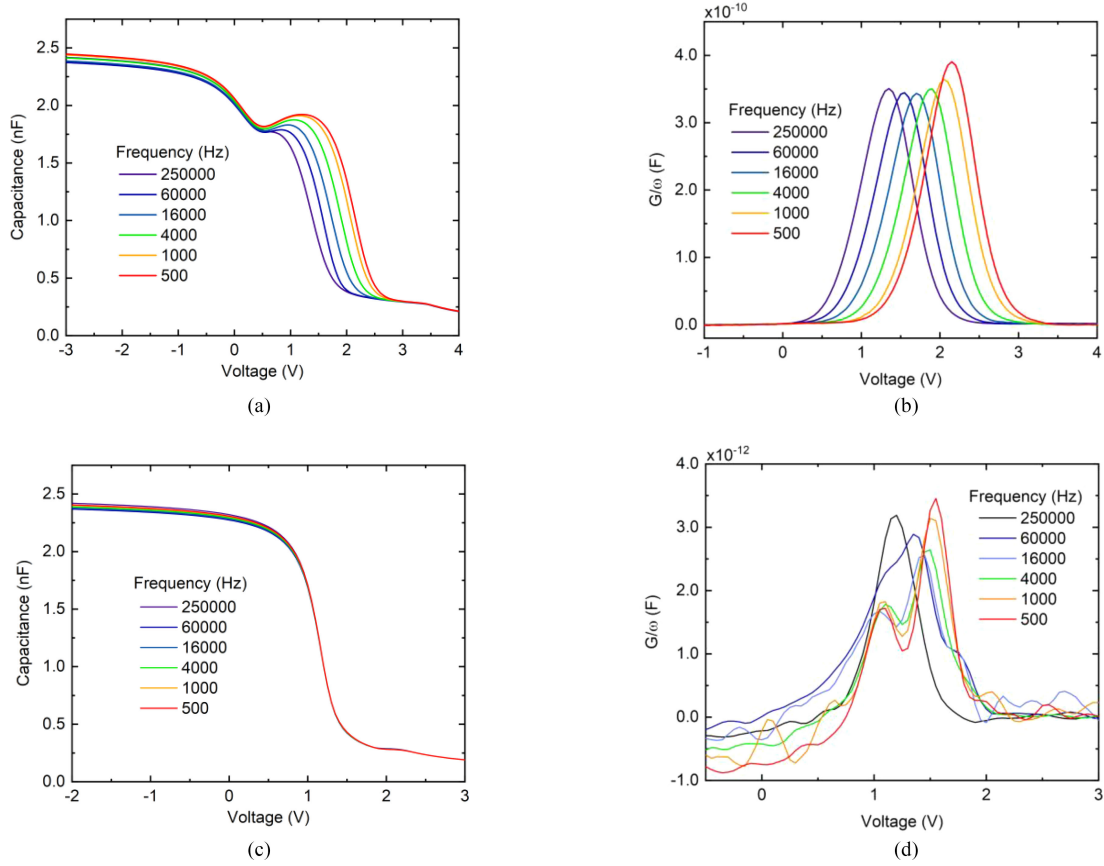


Fig. 5. (a) CV characteristics as-deposited. (b) GV characteristics as-deposited. (c) CV characteristics annealed. (d) GV characteristics annealed, of a no-HF sample deposited at 200 °C.

–100 to –200 mV, indicating significant amounts of positive trapped charge. The annealed samples contain low amounts of interfacial traps and exhibit a hysteresis of <40 mV, indicating a negligible contribution from trapped charges to the total shift in V_{FB} of ca. 2 V relative to built-in potential, φ_{ms} . For the annealed samples the approximation $Q_{\text{eff}}(\text{hf}) \approx Q_{\text{fix}}$ thus appears to be reasonable, while for the as-deposited samples, the large amount of trapped charge results in a slight overestimation of the fixed charge. The obtained values are in agreement with previously reported values of Q_{fix} for Al_2O_3 ($-10^{11-13} \text{ cm}^{-2}$) [3], [17], [24]. D_{it} was determined using the conductance method devised by Hill and Coleman [43]

$$D_{\text{it}} = \frac{2}{qA} \frac{\max\left(\frac{G}{\omega}\right)}{\left(\max\left(\frac{G}{\omega}\right) \frac{1}{C_{\text{ox}}}\right)^2 + \left(1 - \frac{C}{C_{\text{ox}}}\right)^2} \quad (2)$$

where $\max(G/\omega)$ is the peak value of the largest peak in Fig. 5(b) and (d), and C is the corresponding capacitance at that voltage. D_{it} for the as-deposited films deposited at 200 °C was determined to be 2.4×10^{12} and $2.1 \times 10^{12} \text{ eV}^{-1} \text{ cm}^{-2}$ for the HF-dipped and no-HF samples, respectively. The values are in agreement with previously reported values for as-deposited Al_2O_3 [44], [45]. Note that with $\max(G/\omega)$ occurring at the lowest frequency used, i.e. 500 Hz, it is likely that the actual maximum is at a lower frequency, and the reported D_{it} values may thus be slightly underestimated. It is also possible that the

interface state distribution at the Si- Al_2O_3 is particularly low in the lower part of the bandgap that has been probed in this article.

Post annealing, the D_{it} was determined to be 2.8×10^{10} and $9.8 \times 10^9 \text{ eV}^{-1} \text{ cm}^{-2}$ for the HF-dipped and no-HF samples deposited at 200 °C, respectively, with the no-HF sample exhibiting the lowest D_{it} among the samples in this article. The two peaks in the GV characteristics of the annealed no-HF sample (5-D) could be because of two similarly populated defect levels that respond differently to the frequency. The other samples only exhibit one significant peak with $\max(G/\omega)$ at 500 Hz, shown for the samples deposited at 250 °C in Fig. S5. The 500 Hz peak was consequently used for D_{it} extraction for all samples (Fig. S6).

Fig. 6(a) shows the obtained Q_{fix} of all samples, while the corresponding D_{it} of the samples are presented in Fig. 6(b). The exact values are available in Table S3 and S4. The no-HF samples consistently exhibit lower D_{it} values and equal or more Q_{fix} , agreement with the reduced $J_{0\text{s}}$ of no-HF samples relative to HF-dipped samples observed from the PCD measurements in Fig. 3. Fig. 6(b) also shows that D_{it} increases for deposition at temperatures >200 °C. We did not observe any significant changes in the CV or GV characteristics over time for any of the samples. The apparent decrease in Q_{fix} post annealing can be attributed to the overestimation of the Q_{fix} in the as-deposited samples because of trapped negative interfacial charges.

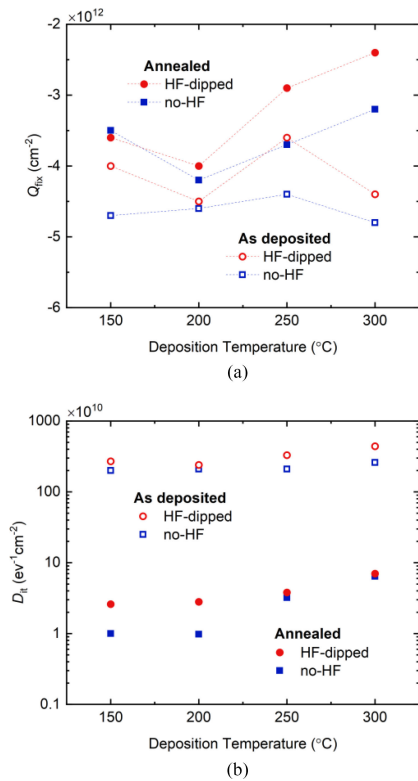


Fig. 6. (a) Q_{fix} and (b) D_{it} for HF-dipped (red) and no-HF (blue) for as-deposited samples (open) and annealed samples (filled), deposited at different temperatures. The 150 $^{\circ}\text{C}$ data points are from [32]. Dashed lines serve as guides for the eye.

IV. DISCUSSION

Both the results from PCD and impedance measurements demonstrate that the no-HF samples exhibit superior surface passivation to the HF-dipped samples when comparing samples deposited at the same deposition temperature. We previously demonstrated this for samples deposited at 150 $^{\circ}\text{C}$ [32], and the present study indicates that this is generally true for deposition temperatures in the 150–300 $^{\circ}\text{C}$ range for the TMA + H₂O + O₃ process. Importantly, this includes depositions at 200 $^{\circ}\text{C}$, previously determined to be the optimal deposition temperature [6], [38], [41], where the no-HF sample exhibits more than three times lower J_{0s} post annealing, which CV and GV characteristics indicate is because of an almost three times lower D_{it} and slightly increased Q_{fix} .

A possible reason for the HF-dipped samples performing worse than the ones with a SiO_x layer is likely related to the differences in the reaction of TMA with Si-H and Si-OH. We previously proposed Al and C may be incorporated into the SiO_x layer that is formed during the initial ALD cycles on H-terminated Si [32]. We will elaborate a bit further on this here.

A key difference in depositing on SiO_x and H-terminated Si is the reaction mechanisms during the initial ALD cycles. Previous studies have shown that while steady-state growth of 4 Al/nm² occurs already after the first ALD cycle on OH-terminated SiO_x, only ca. 0.1 Al/nm² is deposited during the first ALD cycle on H-terminated Si at 300 $^{\circ}\text{C}$, which increases to the steady-state

growth rate after ca. 15–20 cycles [12], [46], [47]. During the first TMA cycle, *in-situ* transmission infra-red spectroscopy has shown only small reductions in Si-H bonds, while significant Si-CH₃ and small amounts of Al-CH₃ bond formation are observed [48]. Only the Al-CH₃ species are reactive toward H₂O, therefore in the subsequent H₂O pulse, Si-Al-OH species are formed only at these locations. The Al-OH species are highly reactive toward TMA, which can result in island growth formation of Al₂O₃, as previously indicated by TEM [47]. Most of the Si-CH₃ species can eventually become hydrolyzed by neighboring Al-OH species once the coverage of Al-OH is large enough [48], and the H-terminated Si may eventually also become oxidized during the H₂O and O₃ pulses. The oxidation of H-terminated Si by H₂O has been studied in detail previously, and it is believed that Si-OH and H₂ are formed initially, and that the OH- group then inserts into a Si-Si back bond, creating Si-O-Si and regenerates a Si-H bond at the surface, which then reacts with more H₂O [49], [50]. The low growth rates are thus likely to result in an AlO_x layer with a different structure and density than an AlO_x layer growing at steady-state growth conditions after the first cycle. The 0.5–2 nm SiO_x layer that is formed during the deposition, as demonstrated by TEM of as-deposited samples [2], [12], [13], is formed while Si-CH₃ and Si-Al-CH₃ are covering the surface, possibly causing both Al and C to be incorporated into the SiO_x layer, likely resulting in increased D_{it} [51]. Annealing should enable the rearrangement of the interface atoms in a way that reduces the high energy associated with dangling bonds and uncompensated charges in the disordered SiO_x-AlO_x layer. This could explain why the lifetime between HF-dipped and no-HF samples differs by more than an order of magnitude as-deposited, while it is much less after annealing. However, annealing may also cause Al to diffuse into the SiO_x layer, particularly if the SiO_x layer is highly disordered [52]. Secondary ion mass spectrometry of an annealed ALD Al₂O₃ film deposited on H-terminated Si has also previously shown that at the depth where 1/3 of the detected atoms are Si, which would be expected from tetrahedrally coordinated Si in SiO₂, 1/5 of the detected atoms are Al, thus revealing large amounts of Al in the SiO_x layer [53]. Electron energy loss spectroscopy measurements have similarly detected the presence of Al all the way down into the Si substrate [54]. As the SiO_x layer of the no-HF samples has not been formed in the presence of Si-Al-CH₃, it likely has a lower aluminum concentration, and possibly lower carbon concentration, depending on the conditions in which the SC2-last SiO_x was formed.

An alternative or complimentary reason for the reduced surface passivation of the HF-dipped samples may be related to differences in hydrogen concentration at the interface. As H-terminated Si is known to be resistant to oxidation, it is possible that less Si-O bonds are formed at the interface during the ALD deposition. When the Si-H bonds break at a later stage, the D_{it} increases [55]. That these bonds can break can also be inferred from the reduced lifetime of <10 nm Al₂O₃ films, which previously been attributed to hydrogen effusion from the interface [56], [57]. As the Si-H bonds dissociate over time, it may consequently be better to wait for this to happen before oxidizing the surface or to grow a thin layer

that minimizes the coverage of Si-H bonds at the interface. However, after the initial Si-O formation, any hydrogen that diffuses toward the interface may passivate leftover dangling bonds and is thus likely to reduce D_{it} further. As these bonds may break again, this improvement may not be permanent, however, increasing Al₂O₃ layer thickness appears to reduce hydrogen effusion, indicating that the Si-H bonds can be stabilized this way [56], [57].

It follows that the increased J_{0s} over time observed for samples deposited below 300 °C in this article could also be related to hydrogen effusion. As Al₂O₃ deposited using H₂O at lower temperatures contains significantly more hydrogen [58], and these samples exhibit the largest increase in J_{0s} over time, a likely explanation for the observations is that more hydrogen effuses away from the interface in samples where the Al₂O₃ layer supplies large amounts of hydrogen to the interface. The lower density of these films also suggest that hydrogen effusion may be more efficient. Samples deposited at 300 °C should contain very low amounts of hydrogen and consequently have a higher mass density, and the improvement observed over time may possibly be attributed to hydrogen trapped in the Al₂O₃ being released and diffusing toward the interface over time. It is our interpretation that a longer annealing step or higher temperature would be beneficial for samples with lower hydrogen concentration and higher mass density.

More research is necessary to completely understand how the SiO_x layer formation influences Q_{fix} and D_{it} . However, the results indicate that an excellent level of surface passivation can be achieved by depositing 20 nm Al₂O₃ using a mixture of H₂O and O₃ at a deposition temperature of 200 °C on ca. 1.6 nm of SC2-last SiO_x. Supported by a J_{0s} of only 0.9 fA/cm² ca. 10 min after annealing for 10 min in FG at 435 °C, which stabilizes 1.2 fA/cm². J_{0s} values have rarely been reported for polished surfaces passivated with Al₂O₃ previously. However, Steinhauser *et al.* [33], recently presented results that indicates a J_{0s} of ca. 1 fA/cm² for the sample with the current highest reported lifetime. They performed extensive pretreatments, including a thin a-SiC_x layer, i.e. the Al₂O₃ was not deposited on H-terminated Si. The results in the present study indicate that a similar level of surface passivation can be achieved by simply depositing Al₂O₃ on the SiO_x that forms during and after chemical mechanical polishing and SC1/SC2 rinsing when using the process presented in this article. The key importance being that the surface should not be H-terminated prior to Al₂O₃ deposition and that a thin layer of e.g. SiO_x or SiC_x significantly reduces D_{it} . A thin SiO_x layer was also previously suggested to be beneficial by Breitenstein *et al.* [30]. To achieve more control of the process, it is our interpretation that an HF-dip followed by SC1/SC2 rinsing and subsequent SiO_x growth in air until ca. 1.5 nm SiO_x has formed, which should yield similar results as those presented in this article. However, the presented results demonstrate that an out-of-the-box oxide in combination with Al₂O₃ can result in excellent surface passivation, supported by the exceptionally low D_{it} and high Q_{fix} of a similarly processed sample. The process that resulted in the lowest J_{0s} in this article thus offers an affordable alternative for achieving a high level of surface passivation.

V. CONCLUSION

We have demonstrated that the TMA + H₂O + O₃ ALD process results in excellent surface passivation of *p*-type Si when followed by FGA at 435 °C for 10 min. The highest level of surface passivation was achieved for a sample where the SC2-last SiO_x layer already present on the wafer was not removed prior to Al₂O₃ deposition carried out at 200 °C, resulting in J_{0s} of 0.9 fA/cm² shortly after annealing, which had increased to 1.2 fA/cm² after 8 months of storage. CV and GV revealed that the sample processed in the same way exhibited the lowest D_{it} of 9.8×10^9 eV⁻¹ cm⁻² and the highest Q_{fix} of -4.2×10^{12} cm⁻² among the annealed samples investigated in this article. For every deposition temperature, samples subjected to a 3 min HF-dip consistently exhibited higher J_{0s} and D_{it} than samples where the SC2-last SiO_x layer was not removed prior to deposition. We propose that H-terminated Si may impede Si-O bond formation during deposition, and subsequent hydrogen effusion results in increased D_{it} .

Most of the samples deposited at 150 and 200 °C exhibited a ca. 50% increase in J_{0s} after 8 months of cleanroom storage after annealing, while for samples deposited at higher temperatures, either a minor increase or a significant decrease was observed. Because of the low initial J_{0s} of samples deposited at 200 °C, these samples still exhibited significantly lower J_{0s} compared with similarly processed samples deposited at other temperatures. The observed differences in long-term stability are proposed to related to the hydrogen concentration in the Al₂O₃ layers.

ACKNOWLEDGMENT

A CC BY or equivalent license is applied to any Author Accepted Manuscript (AAM) version arising from this submission, in accordance with the grant's open access conditions.

REFERENCES

- [1] M. Fischer, M. Woodhouse, S. Herritsch, and J. Trube, *VDMA Photovoltaic Equipment*. Frankfurt am Main, Germany: International Technology Roadmap for Photovoltaic, 2000.
- [2] B. Hoex, S. B. S. Heil, E. Langereis, M. C. M. van Den Sanden, and W. M. M. Kessels, "Ultralow surface recombination of C-Si substrates passivated by plasma-assisted atomic layer deposited Al₂O₃," *Appl. Phys. Lett.*, vol. 89, 2006, Art. no. 042112.
- [3] G. Dingemans and W. M. M. Kessels, "Status and prospects of Al₂O₃-based surface passivation schemes for silicon solar cells," *J. Vac. Sci. Technol. A*, vol. 30, 2012, Art. no. 040802.
- [4] J. Schmidt, B. Veith, and R. Brendel, "Effective surface passivation of crystalline silicon using ultrathin Al₂O₃ films and Al₂O₃/SiNx stacks," *Phys. Status Solidi Rapid Res. Lett.*, vol. 3, pp. 287–289, 2009.
- [5] D. K. Simon *et al.*, "Symmetrical Al₂O₃-based passivation layers for P- and N-type silicon," *Sol. Energy Mater. Sol. Cells*, vol. 131, pp. 72–76, 2014.
- [6] N. Batra, J. Gope, J. P. Vandana, R. Singh, and P. Singh, "Influence of deposition temperature of thermal ALD deposited Al₂O₃ films on silicon surface passivation," *AIP Adv.*, vol. 5, 2015, Art. no. 067113.
- [7] R. S. Bonilla, B. Hoex, P. Hamer, and P. R. Wilshaw, "Dielectric surface passivation for silicon solar cells: A review," *Phys. Status Solidi A*, vol. 214, 2017, Art. no. 1700293.
- [8] J. Schmidt, R. Peibst, and R. Brendel, "Surface passivation of crystalline silicon solar cells: Present and future," *Sol. Energy Mater. Sol. Cells*, vol. 187, pp. 39–54, 2018.

- [9] J. Schmidt *et al.*, "Progress in the surface passivation of silicon solar cells," in *Proc. 23rd Eur. Photovolt. Sol. Energy Conf.*, 2008, pp. 974–981.
- [10] G. Dingemans *et al.*, "Stability of Al_2O_3 and $\text{Al}_2\text{O}_3/\text{a-SiNx:H}$ stacks for surface passivation of crystalline silicon," *J. Appl. Phys.*, vol. 106, 2009, Art. no. 114907.
- [11] O. A. Dicks, J. Cottom, A. L. Shluger, and V. V. Afanas'ev, "The origin of negative charging in amorphous Al_2O_3 films: The role of native defects," *Nanotechnology*, vol. 30, 2019, Art. no. 205201.
- [12] A. Delabie *et al.*, "Reaction mechanisms for atomic layer deposition of aluminum oxide on semiconductor substrates," *J. Vac. Sci. Technol. A*, vol. 30, 2011, Art. no. 01A127.
- [13] D.-H. Kim, S.-B. Baek, and Y.-C. Kim, "Energy barriers for trimethylaluminum reaction with varying surface hydroxyl density," *Appl. Surf. Sci.*, vol. 258, pp. 225–229, 2011.
- [14] D. Hiller *et al.*, "Deactivation of silicon surface states by Al-induced acceptor states from Al–O monolayers in SiO_2 ," *J. Appl. Phys.*, vol. 125, 2019, Art. no. 015301.
- [15] D. König, D. Hiller, S. Gutsch, M. Zacharias, and S. Smith, "Modulation doping of silicon using aluminium-induced acceptor states in silicon dioxide," *Sci. Rep.*, vol. 7, 2017, Art. no. 46703.
- [16] B. Hoex *et al.*, "Excellent passivation of highly doped p-type Si surfaces by the negative-charge-dielectric Al_2O_3 ," *Appl. Phys. Lett.*, vol. 91, 2007, Art. no. 112107.
- [17] D. K. Simon, P. M. Jordan, T. Mikolajick, and I. Dirnstorfer, "On the control of the fixed charge densities in Al_2O_3 -based silicon surface passivation schemes," *ACS Appl. Mater. Interfaces*, vol. 7, pp. 28215–28222, 2015.
- [18] T. Niewelt *et al.*, "Taking monocrystalline silicon to the ultimate lifetime limit," *Sol. Energy Mater. Sol. Cells*, vol. 185, pp. 252–259, 2018.
- [19] A. Cuevas and D. Yan, "Misconceptions and misnomers in solar cells," *IEEE J. Photovolt.*, vol. 3, no. 2, pp. 916–923, Apr. 2013.
- [20] B. Hoex, J. J. H. Gielis, M. C. M. V. D. Sanden, and W. M. M. Kessels, "On the C-Si surface passivation mechanism by the negative-charge-dielectric Al_2O_3 ," *J. Appl. Phys.*, vol. 104, 2008, Art. no. 113703.
- [21] H. Lee *et al.*, "Interface engineering for the passivation of c-Si with O_3 -based atomic layer deposited AlO_x for solar cell application," *Appl. Phys. Lett.*, vol. 100, 2012, Art. no. 143901.
- [22] G. Dingemans *et al.*, "Influence of the oxidant on the chemical and field-effect passivation of Si by ALD Al_2O_3 ," *Electrochemistry Solid-State Lett.*, vol. 14, pp. H1–H4, 2011.
- [23] G. von Gastrow *et al.*, "Effect of ozone concentration on silicon surface passivation by atomic layer deposited Al_2O_3 ," *Appl. Surf. Sci.*, vol. 357, pp. 2402–2407, 2015.
- [24] G. Dingemans, N. M. Terlinden, M. A. Verheijen, M. C. M. V. D. Sanden, and W. M. M. Kessels, "Controlling the fixed charge and passivation properties of $\text{Si}(100)/\text{Al}_2\text{O}_3$ interfaces using ultrathin SiO_2 interlayers synthesized by atomic layer deposition," *J. Appl. Phys.*, vol. 110, 2011, Art. no. 093715.
- [25] A. Laades *et al.*, "On the impact of interfacial SiO_x -layer on the passivation properties of PECVD synthesized aluminum oxide," *Physica Status Solidi C*, vol. 9, pp. 2120–2123, 2012.
- [26] A. Moldovan *et al.*, "Simple cleaning and conditioning of silicon surfaces with UV/ozone sources," *Energy Procedia*, vol. 55, pp. 834–844, 2014.
- [27] L. E. Black *et al.*, "Explorative studies of novel silicon surface passivation materials: Considerations and lessons learned," *Sol. Energy Mater. Sol. Cells*, vol. 188, pp. 182–189, 2018.
- [28] H. Angermann, "Conditioning of Si-interfaces by wet-chemical oxidation: Electronic interface properties study by surface photovoltage measurements," *Appl. Surf. Sci.*, vol. 312, pp. 3–16, 2014.
- [29] Y. Bao *et al.*, "Effect of substrate pretreatments on the atomic layer deposited Al_2O_3 passivation quality," *J. Vac. Sci. Technol. A*, vol. 33, 2015, Art. no. 01A123.
- [30] L. Breitenstein, A. Richter, M. Hermle, and W. Warta, "Studies on wet-chemical surface conditioning for Al_2O_3 passivation layers deposited with ALD," in *Proc. 26th Eur. Photovolt. Sol. Energy Conf. Exhib.*, 2011, pp. 2247–2251.
- [31] K. R. McIntosh and L. E. Black, "On effective surface recombination parameters," *J. Appl. Phys.*, vol. 116, 2014, Art. no. 014503.
- [32] M. N. Getz, M. Povoli, and E. Monakhov, "Effect of the native oxide on the surface passivation of Si by Al_2O_3 ," *J. Appl. Phys.*, vol. 129, 2021, Art. no. 205701.
- [33] B. Steinhäuser, T. Niewelt, A. Richter, R. Eberle, and M. C. Schubert, "Extraordinarily high minority charge carrier lifetime observed in crystalline silicon," *Sol. RRL*, vol. 5, 2021, Art. no. 2100605.
- [34] L. E. Black, T. Allen, K. R. McIntosh, and A. Cuevas, "Effect of boron concentration on recombination at the P-Si– Al_2O_3 interface," *J. Appl. Phys.*, vol. 115, 2014, Art. no. 093707.
- [35] C. M. Herzinger, B. Johs, W. A. McGahan, J. A. Woollam, and W. Paulson, "Ellipsometric determination of optical constants for silicon and thermally grown silicon dioxide via a multi-sample, multi-wavelength, multi-angle investigation," *J. Appl. Phys.*, vol. 83, pp. 3323–3336, 1998.
- [36] F. Campabadal, O. Beldarrain, M. Zabalá, M. C. Acero, and J. M. Rafi, "Comparison between Al_2O_3 thin films grown by ALD using H_2O or O_3 as oxidant source," in *Proc. 8th Spanish Conf. Electron Devices*, 2011, pp. 1–4.
- [37] S. E. Potts, G. Dingemans, C. Lachaud, and W. M. M. Kessels, "Plasma-enhanced and thermal atomic layer deposition of Al_2O_3 using dimethylaluminum isopropoxide, $[\text{Al}(\text{CH}_3)_2(\mu\text{-O}i\text{Pr})_2]$, as an alternative aluminum precursor," *J. Vac. Sci. Technol. A*, vol. 30, 2012, Art. no. 021505.
- [38] H. Huang *et al.*, "Data of ALD Al_2O_3 rear surface passivation, Al_2O_3 PERC cell performance, and cell efficiency loss mechanisms of Al_2O_3 PERC cell," *Data Brief*, vol. 11, pp. 19–26, 2017.
- [39] D. E. Kane and R. Swanson, "Measurement of the emitter saturation current by a contactless photoconductivity decay method," in *Proc. 18th IEEE Photovolt. Specialists Conf.*, 1985, Art. no. 578.
- [40] A. Richter, S. W. Glunz, F. Werner, J. Schmidt, and A. Cuevas, "Improved quantitative description of Auger recombination in crystalline silicon," *Phys. Rev. B*, vol. 86, 2012, Art. no. 165202.
- [41] G. Dingemans, M. C. M. van den Sanden, and W. Kessels, "Influence of the deposition temperature on the C-Si surface passivation by Al_2O_3 films synthesized by ALD and PECVD," *Electrochem. Solid-State Lett.*, vol. 13, 2010, Art. no. 165202.
- [42] J. A. Töfflinger *et al.*, "PECVD- AlO_x/SiNx passivation stacks on silicon: Effective charge dynamics and interface defect state spectroscopy," *Energy Procedia*, vol. 55, pp. 845–854, 2014.
- [43] W. A. Hill and C. C. Coleman, "A single-frequency approximation for interface-state density determination," *Solid-State Electron.*, vol. 23, pp. 987–993, 1980.
- [44] R. Hezel and K. Jaeger, "Low-temperature surface passivation of silicon for solar cells," *J. Electrochem. Soc.*, vol. 136, pp. 518–523, 1989.
- [45] J. Benick *et al.*, "Effect of a post-deposition anneal on $\text{Al}_2\text{O}_3/\text{Si}$ interface properties," in *Proc. 35th IEEE Photovolt. Specialists Conf.*, 2010, pp. 000891–000896.
- [46] R. L. Puurunen, "Surface chemistry of atomic layer deposition: A case study for the trimethylaluminum/water process," *J. Appl. Phys.*, vol. 97, 2005, Art. no. 121301.
- [47] R. L. Puurunen *et al.*, "Island growth in the atomic layer deposition of zirconium oxide and aluminum oxide on hydrogen-terminated silicon: Growth mode modeling and transmission electron microscopy," *J. Appl. Phys.*, vol. 96, pp. 4878–4889, 2004.
- [48] M. M. Frank *et al.*, "Enhanced initial growth of atomic-layer-deposited metal oxides on hydrogen-terminated silicon," *Appl. Phys. Lett.*, vol. 83, pp. 740–742, 2003.
- [49] D. D. M. Wayner and R. A. Wolkow, "Organic modification of hydrogen terminated silicon surfaces1," *J. Chem. Soc., Perkin Trans.*, vol. 2, pp. 23–34, 2002.
- [50] B. Gokce, E. J. Adles, D. E. Aspnes, and K. Gundogdu, "Measurement and control of in-plane surface chemistry during the oxidation of H-terminated (111) Si," *Nat. Acad. Sci.*, vol. 107, pp. 17503–17508, 2010.
- [51] S. W. Lim, F. Machuca, H. Liao, R. P. Chiarello, and R. C. Helms, "Effect of initial Al contamination on ultrathin gate oxides," *J. Electrochem. Soc.*, vol. 147, 2000, Art. no. 1136.
- [52] N. E. Grant *et al.*, "Atomic level termination for passivation and functionalisation of silicon surfaces," *Nanoscale*, vol. 12, pp. 17332–17341, 2020.
- [53] Z. Chen *et al.*, "Study of gamma-ray radiation effects on the passivation properties of atomic layer deposited Al_2O_3 on silicon using deep-level transient spectroscopy," *J. Mater. Sci.: Mater. Electron.*, vol. 30, pp. 1148–1152, 2019.
- [54] K. Kimoto *et al.*, "Coordination and interface analysis of atomic-layer-deposition Al_2O_3 on Si(001) using energy-loss near-edge structures," *Appl. Phys. Lett.*, vol. 83, pp. 4306–4308, 2003.
- [55] M. Jech *et al.*, "Quantum chemistry treatment of silicon-hydrogen bond rupture by nonequilibrium carriers in semiconductor devices," *Phys. Rev. Appl.*, vol. 16, 2021, Art. no. 014026.
- [56] F. Werner *et al.*, "Electronic and chemical properties of the c-Si/ Al_2O_3 interface," *J. Appl. Phys.*, vol. 109, 2011, Art. no. 113701.
- [57] S. Banerjee and M. K. Das, "A review of Al_2O_3 as surface passivation material with relevant process technologies on C-Si solar cell," *Opt. Quantum Electron.*, vol. 53, 2021, Art. no. 60.
- [58] M. Groner, F. Fabreguette, J. Elam, and S. M. George, "Low-temperature Al_2O_3 atomic layer deposition," *Chem. Mater.*, vol. 16, pp. 639–645, 2004.